ChemPubSoc Europe

DOI: 10.1002/celc.201801088

CHEMELECTROCHEM Articles

Lithiation and Delithiation Reactions of Binary Silicide Electrodes in an Ionic Liquid Electrolyte as Novel Anodes for Lithium-Ion Batteries

Yasuhiro Domi,[a, c, d] Hiroyuki Usui,[a, c, d] Rena Takaishi,[b, c, d] and Hiroki Sakaguchi*[a, c, d]

We investigated the lithiation and delithiation properties of pure binary silicide electrodes in an ionic liquid electrolyte as novel anodes for lithium-ion batteries. Some electrodes maintain a high reversible capacity in the electrolyte, whereas they show a poor cycling performance in an organic electrolyte. The superior performance results from the high affinity for the transition metal that composes the silicide with Li. Based on reaction behavior analysis, the crystal structure of silicide is maintained during the cycling, and phase separation does not occur. The ionic liquid electrolyte suppresses the formation of cracks and exfoliation of the silicide layer from a substrate. In addition, a surface film formed on the silicide electrode through the reductive decomposition of the electrolyte has different components than that on a Si electrode, even in the same ionic liquid electrolyte. Soft X-ray emission spectroscopy demonstrates that the pure silicide itself reacts with Li. The obtained results will provide significant insights into novel alloy-based anode materials for lithium-ion batteries.

1. Introduction

Developing lithium-ion batteries (LIBs) that have high energy density and a long cycle life is important to building a sustainable society because LIBs are used as electric vehicle batteries and stationary batteries for utilizing renewables.[1,2] Si has great potential as an anode active material for next-generation LIBs because its theoretical capacity (3580 $mA\,h\,g^{-1}$ for $Li_{15}Si_4$) is approximately ten times higher than that of graphite (372 $mA\,h\,g^{-1}$ for LiC_6), which is currently used.[3] However, Si electrodes show poor cycle stability, which is mainly caused by a large volume change in Si during the alloying (charge) and dealloying (discharge) reactions with Li. In addition, Si has other disadvantages, such as high electrical resistivity and a low Li^+ diffusion coefficient.

Many research groups have put significant efforts into these issues: coating Si with conductive materials to reduce the electrical resistivity,[4] synthesizing nanostructured Si materials to cushion volume expansion,[5,6] doping Si with impurities to increase its electrical conductivity and/or suppress its phase transition from Si to crystalline $Li_{15}Si_4$ phases.[7,8] We have previously reported that a composite electrode that consisted of elemental Si and a binary silicide (M_ySi_z, *M*: metal), such as $LaSi_2$ and Gd–Si, shows a superior electrochemical performance in conventional organic electrolytes compared to the Si-alone electrode.[9,10] While the reversible capacity of silicide-alone electrodes is much lower than that of a Si electrode in organic electrolytes,[9–12] the electrochemical performance of the composite electrode is mainly affected by the four properties of silicide: (1) mechanical properties to release the stress from Si, (2) low electronic resistivity, (3) moderate reactivity with Li^+, and (4) high thermodynamic stability.

The electrolyte contributes to the performance and safety of LIBs.[13,14] An increase in the energy density of LIBs leads to a greater probability of combustion; hence, non-flammable electrolytes should be used to enhance the safety of LIBs. Ionic liquids have excellent physicochemical properties as electrolyte solvents, such as negligible vapor pressure, non-flammability, high conductivity, and wide electrochemical windows.[15–18] We have reported that a Si-anode exhibits a better electrochemical performance in some ionic liquid electrolytes compared to that in conventional organic electrolytes.[19–21] In addition, we have applied the ionic liquid electrolytes to the composite electrodes. As a result, some ionic electrolytes contribute to improving the cyclability of the composite electrode compared to the organic electrolytes, but others deteriorate the performance.[21,22] To reveal the difference in the performance of the composite electrode in the ionic liquid electrolytes, it is important to elucidate the reaction behavior of silicide-alone electrodes in the electrolytes.

Lithiation and delithiation properties of silicides have not yet been investigated in ionic liquid electrolytes. On the other

[a] Dr. Y. Domi, Dr. H. Usui, Prof. H. Sakaguchi
Department of Chemistry and Biotechnology, Graduate School of Enginnering, Tottori University, 4-101 Minami, Koyama-cho, Tottori 680–8552, Japan
E-mail: sakacuhi@tottori-u.ac.jp
[b] R. Takaishi
Graduate School of Sustainability Science, Tottori University, 4–101 Minami, Koyama-cho, Tottori 680–8552, Japan
[c] Dr. Y. Domi, Dr. H. Usui, R. Takaishi, Prof. H. Sakaguchi
Center for Research on Green Sustainable Chemistry, Tottori University, 4–101 Minami, Koyama-cho, Tottori 680–8552, Japan
[d] Dr. Y. Domi, Dr. H. Usui, R. Takaishi, Prof. H. Sakaguchi
Global Research Center for Environment and Energy based on Nanomaterials Science, National Institute for Materials Science, Namiki 1–1, Tsukuba, Ibaraki 305–0044, Japan

Supporting information for this article is available on the WWW under https://doi.org/10.1002/celc.201801088

hand, in organic electrolytes, some groups have reported the charge-discharge properties of some silicides.[23–26] However, the groups have performed insufficient characterization: they characterized prepared samples by only X-ray diffraction (XRD), which detects the crystalline material but cannot detect amorphous ones. Assuming that the synthesized samples include amorphous Si (*a*-Si), an estimated reversible capacity should largely differ. Although the groups proposed reaction mechanisms of silicide with Li, they did not demonstrate the mechanism on the basis of experimental results. Other groups have synthesized various M_ySi_{1-y} and have revealed that two phases of Si and certain silicides co-exist in the resulting M_ySi_{1-y}.[27–33] They have investigated the charge-discharge properties of a mixture of Si and a certain silicide.

In this study, it is important to prepare silicide-alone phases. Here, we synthesized various pure binary silicide powders and carefully characterize them by XRD and Raman spectroscopy, which detects *a*-Si in addition to crystalline Si (*c*-Si). We also investigated their lithiation and delithiation properties of silicides in an ionic liquid electrolyte as novel anode for LIBs and determine their reaction behavior with respect to phase transition, change in morphology, and reactivity with Li.

2. Results and Discussion

2.1. Synthesis and Characterization of Various Silicide Powders

We synthesized various silicide powders by a mechanical alloying (MA) method (see the experimental section). Table 1 summarizes an optimized mixture ratio of raw materials, rotary speed, and treatment time for MA. Figure 1a shows the XRD pattern of powder synthesized from Cr and Si powders. Compared with the ICSD patterns, all peaks are assigned to $CrSi_2$, and there are no peaks of the raw materials (Cr and Si), which indicates that the crystalline $CrSi_2$ phase forms. Other crystalline M_ySi_z phases are also obtained, as shown in Figure 1b-f. Figure 2 provides the Raman spectra of all synthesized silicides. Peaks assigned to *c*-Si and *a*-Si appear at approximately 520 and 490 cm^{-1}, respectively.[19,20] Each silicide also gives no Raman peaks which indicates that neither *c*-Si nor *a*-Si is included in the synthesized powders. Therefore, the MA treatment successfully produces a pure silicide phase. For $FeSi_2$ and $LaSi_2$, the mixture ratio differs from the stoichiometric ratio (Table 1). We confirmed the identity of the residue on the ball and/or inside the wall of the pod after the synthesis. Excess Si or La would be included in the scaffolding because these raw materials were not detected in the XRD patterns and Raman spectra.

Table 1. MA conditions for synthesis of each silicide.

M in M_ySi_z	M:Si (molar ratio)	Rotary speed [rpm]	Time [h]
Cr	1:2	380	10
Mn	11:19	500	20
Fe	1:3	380	70
Ni	1:2	380	30
Cu	3:1	380	15
La	11:20	380	10

2.2. Electrochemical Performance of Silicide Electrodes

Figure 3 shows charge-discharge curves of various silicide electrodes in 1 mol dm^{-3} (M) lithium bis(fluorosulfonyl)amide (LiFSA) in *N*-methyl-*N*-propylpyrrolidinium bis(fluorosulfonyl) amide (Py13-FSA). The silicide electrodes were prepared by a gas deposition (GD) method, which does not require a conductive agent and binder. Because the active material includes neither *c*-Si nor *a*-Si, as shown in Figures 1 and 2, all the capacities result from the lithiation and delithiation reactions of the pure silicides. Due to the reductive decomposition of the electrolyte, the first charge curve of each electrode differs from the second charge curve. On the other hand, the discharge curve is almost the same between the first and second cycles. These results indicate that the charge-discharge reactions of silicide electrodes occur reversibly. The $CrSi_2$, $Mn_{11}Si_{19}$, and $LaSi_2$ electrodes exhibit no obvious potential plateaus in the second cycle. In contrast, $FeSi_2$, $NiSi_2$, and Cu_3Si electrodes have an inclined potential plateau at approximately 0.2 V on charge curve and exhibit a potential slope between 0.3 and 0.7 V on discharge curve. The first Coulombic efficiency widely differs between electrodes, which indicates that the formation process of a surface film depends on the kind of electrode. The process should be intricately influenced by the decomposition potential of the electrolyte, reactivity of the electrodes with electrolyte, and so on. Table S1 summarizes the amount of Li combined with each silicide (x in $Li_xM_ySi_z$), which is calculated from the initial discharge capacity. To determine a precise value of x in $Li_xM_ySi_z$, we must analyze the $Li_xM_ySi_z$ structure using neutron diffraction.

Figure 4a shows the dependence of the gravimetric discharge capacity of various silicide electrodes on the cycle number in 1 M LiFSA/Py13-FSA. The result of $NiSi_2$ and $FeSi_2$ electrodes in 1 M lithium bis(trifluoromethanesulfonyl)amide (LiTFSA)/propylene carbonate (PC) is also shown. In an organic electrolyte (LiTFSA/PC), a discharge capacity of $FeSi_2$ and $NiSi_2$ electrodes rapidly fades. In contrast, in the ionic liquid electrolyte (LiFSA/Py13-FSA), the electrodes maintain high reversible capacity over a long cycle. A surface film is widely accepted to form through the reductive decomposition of the electrolyte. We have previously reported that the thickness of the film formed on the Si-alone electrode is inhomogeneous in PC-based organic electrolytes.[19,20] Li^+ should be preferentially stored in the electrode through not the thicker parts but the thinner parts of the film, because the thicker parts inhibit the lithiation reaction of Si. As a result, extreme volume expansion and contraction occur in local regions of the Si, which generates a high stress and large strain in the active material. The strain accumulates under repeated charge-discharge cycling and causes severe disintegration of the electrode, which results in poor cycle stability. In contrast, a surface film derived from ionic liquid electrolytes is homogeneous and thin. The lithiation of Si

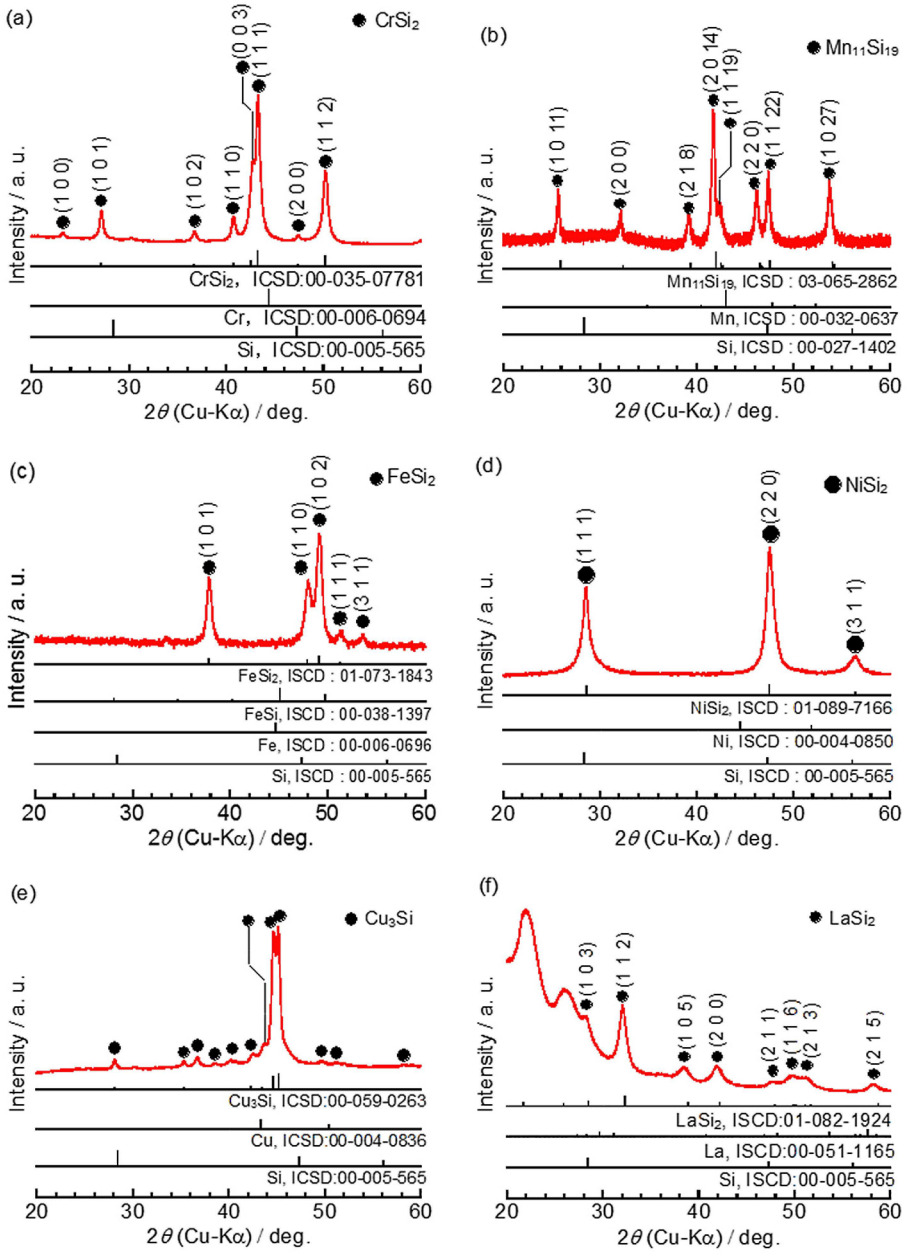

Figure 1. XRD patterns of powders synthesized from various transition metal and Si. The Miller index of Cu_3Si is cited from Ref. [34].

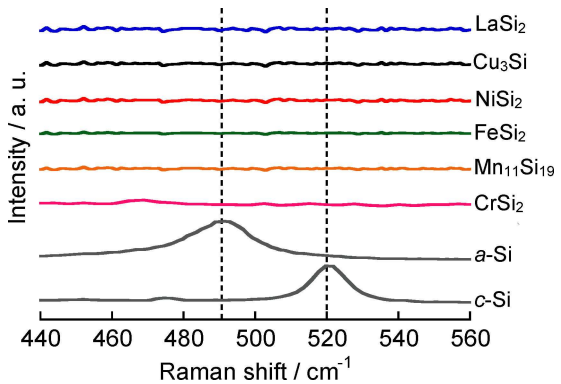

Figure 2. Raman spectra of each silicide electrode. For comparison, the spectra of *c*-Si and *a*-Si are also shown.

uniformly occurs in the ionic liquid electrolytes, which leads to the spread of the stress over the entire electrode surface.[20] No accumulation of strain suppresses the severe disintegration of the Si electrode. It is considered that similar surface films form on the silicide electrode depending on the electrolyte. Therefore, the difference of the cycle performance in the organic and ionic liquid electrolytes is attributed to the difference in properties of the surface films formed on the electrodes. The electrode disintegration is discussed later based on FE-SEM observation.

The discharge capacity of each electrode also differs depending on the transition metal that make up silicide (Figure 4a). The $NiSi_2$ electrode exhibits the highest capacity of approximately 800 mA h g^{-1}, $FeSi_2$ and Cu_3Si electrodes have the

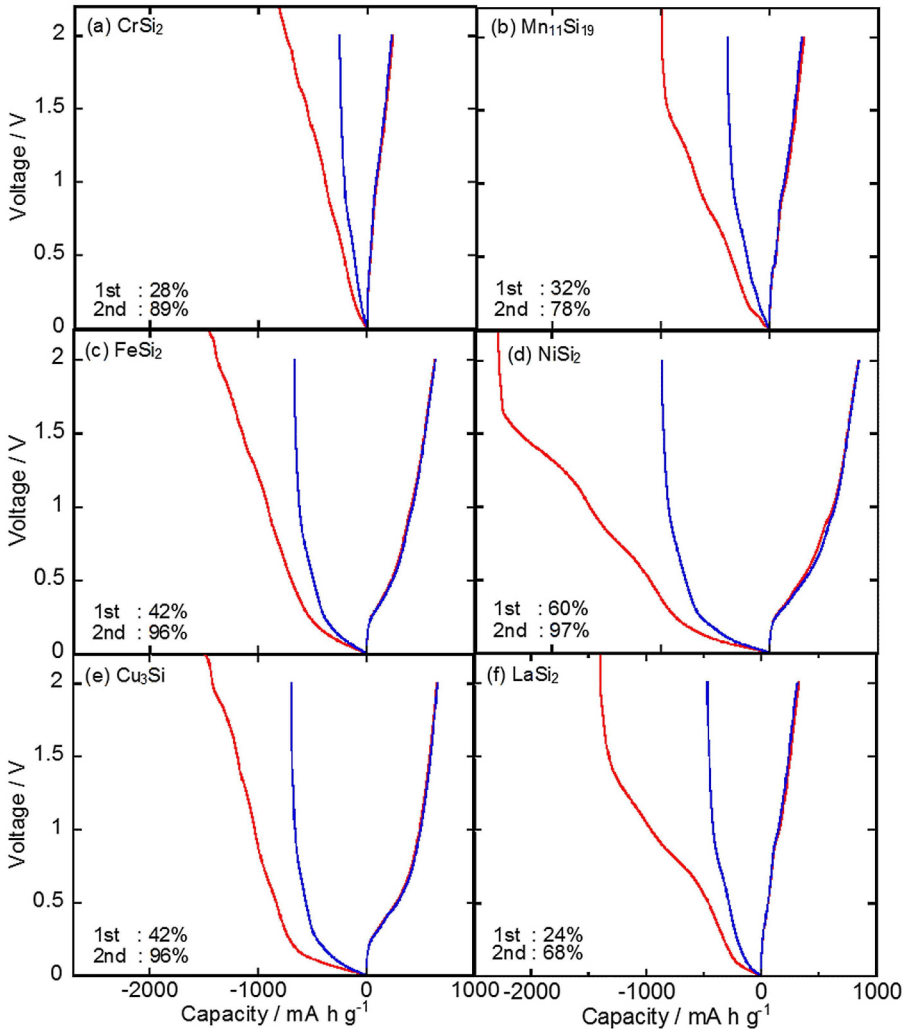

Figure 3. Charge-discharge curves of a) $CrSi_2$, b) $Mn_{11}Si_{19}$, c) $FeSi_2$, d) $NiSi_2$, e) Cu_3Si and f) $LaSi_2$ electrodes in 1 M LiFSA/Py13-FSA. Red and blue lines denote the 1st and 2nd cycles, respectively. The coulombic efficiency is inserted at left below.

middle capacity of approximately 600 mA h g^{-1}, and the other three electrodes have lower capacities, less than 400 mA h g^{-1}. To reveal the difference in discharge capacity, we determined the charge density of each element in $Li_{0.25}MSi_2$ (*M*=Ni, Fe, and La) based on computational chemistry, as shown in Table 2. Figure S1 illustrates the corresponding charge density distribution and crystal structures of $Li_{0.25}MSi_2$. The lattice constants of MSi_2 and $Li_{0.25}MSi_2$ (*M*=Ni, Fe, and La) are shown in Table S2. Li has a positive charge in all silicides, whereas Si, Ni, and Fe have negative charges in $Li_{0.25}LaSi_2$, $Li_{0.25}NiSi_2$, and $Li_{0.25}FeSi_2$, respectively. These results indicate that Li has a high affinity with Si, Ni, and Fe in $Li_{0.25}LaSi_2$, $Li_{0.25}NiSi_2$, and $Li_{0.25}FeSi_2$, respectively.[10] In addition, the higher the affinity of *M* with Li is (the more negative the charge density of *M* is), the higher the discharge capacity is; the discharge capacity correlates with the charge density of *M*.

Table 2. Charge density in $Li_{0.25}MSi_2$ (M = Ni, Fe and La).

	Li	Si	*M*
$Li_{0.25}NiSi_2$	+0.78	+0.40	−1.00
$Li_{0.25}FeSi_2$	+0.57	+0.04	−0.38
$Li_{0.25}LaSi_2$	+0.75	−0.70	+1.21

The volumetric capacity is also important since the battery size is predetermined for ordinary applications. Figure 4b displays dependence of volumetric discharge capacity of various silicide electrodes on cycle number in the ionic liquid electrolyte. For comparison, the result of the Si-alone electrode and theoretical volumetric capacity of graphite electrode are also shown. Note that current rate of the Si-alone electrode differs from that of the silicide electrode. The gravimetric capacity is shown per mass of the un-lithiated material, and the volumetric capacity is usually shown per volume of the fully lithiated material.[35,36] However, the precise *x* in $Li_xM_ySi_z$ is unclear yet, as mentioned above. Hence, the volumetric discharge capacity per mass of the un-lithiated silicide is shown here. Based on the density of graphite (2.25 g cm^{-3}) and silicon (2.33 g cm^{-3}), approximate theoretical volumetric capacity values of graphite and silicon are 837 and 8340 mA h cm^{-3}, respectively.[37,38] Because the density of silicides is larger than

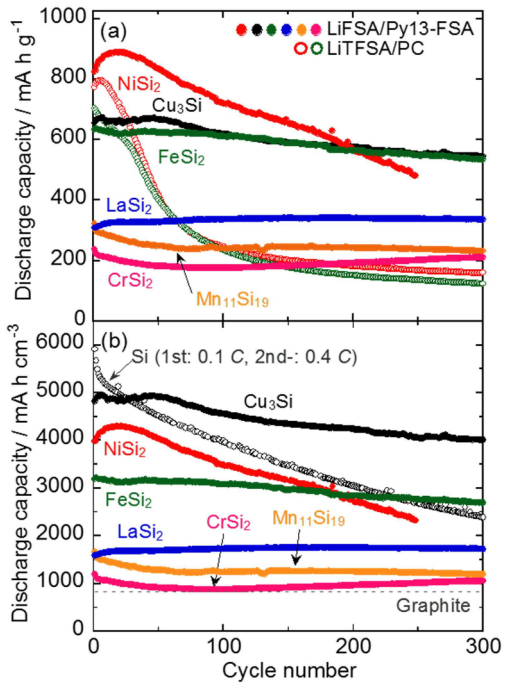

Figure 4. Dependence of a) gravimetric and b) volumetric discharge capacity of various silicide electrodes under the current rate of 50 mA g^{-1} on the cycle number in 1 M LiFSA/Py13-FSA. The results in 1 M LiTFSA/PC are also shown.

that of graphite and silicon, as shown in Table S3,[39] the volumetric discharge capacity of all the silicide electrodes exceeds the approximate theoretical volumetric capacity of graphite. The volumetric capacity of the Si-alone electrode gradually faded and achieved about 2400 mA h cm^{-3} at the 300th cycle. In contrast, the Cu_3Si electrode exhibited a high volumetric capacity of ca. 5000 mA h cm^{-3} at the initial cycle and maintained ca. 4000 mA h cm^{-3} even at the 300th cycle. The $FeSi_2$ electrode also showed ca. 2700 mA h cm^{-3} at the 300th cycle.

Figure S2 shows the dependence of capacity retention of various silicide electrodes in the ionic liquid electrolyte on the cycle number. In contrast, the capacity retention of the Si-alone electrode was approximately 40% at the 300th cycle, $CrSi_2$, $FeSi_2$, Cu_3Si, and $Mn_{11}Si_{19}$ electrodes showed relatively high retention values of 89, 85, 83, and 72%, respectively. An initial increase in the capacity retention of $NiSi_2$ and $LaSi_2$ was confirmed, which indicates an activation process of these silicides. While the former shows retention fading which should result from the electrode disintegration, the later maintains high capacity retention. Consequently, a combination of silicide electrodes and ionic liquid electrolytes have great potential as novel alloy-based anodes in LIBs. Cu_3Si and $FeSi_2$ electrodes are particularly promising anodes from the perspective of high gravimetric and volumetric capacities and great capacity retention.

2.3. Reaction Behavior of Silicide Electrodes

We investigated the phase transition during charge-discharge tests. Figures 5a shows the XRD patterns of lithiated $FeSi_2$ electrodes after 1 and 50 cycles. All peaks are assigned to the $FeSi_2$ phase after the cycling, and no new peaks assigned to Si, Fe, FeSi, and $Li_{15}Si_4$ phases appear.[40] These results demonstrate that the crystal structure of $FeSi_2$ was maintained after charge-discharge tests and indicate that no phase separation of the $FeSi_2$ into Si, Fe, and/or FeSi occurred. We also measured Raman spectra to obtain conclusive evidence of the lack of phase separation (Figure 5b). As a result, no peak assigned to *c*-Si or *a*-Si appears regardless of the electrolyte: no phase separation of the $FeSi_2$ certainly occurred. It is expected that $FeSi_2$ itself reacts with Li (discussed later).

To elucidate the change in the morphology of the $FeSi_2$ electrode, we observed the surface and a cross-section of the electrode by field emission scanning electron microscope (FE–SEM). Figure 6 displays FE-SEM images of the surface and a cross-section of the $FeSi_2$ electrodes. We performed cell disassembly, focused-ion beam (FIB) or cross-section polisher (CP) processes, and FE-SEM observation a few days after the last charge (Figure 6b, c, e, f). To verify the self-discharge progression of the cells (delithiation from the Li-silicide alloy phase), we determined the open circuit voltage (OCV) of the

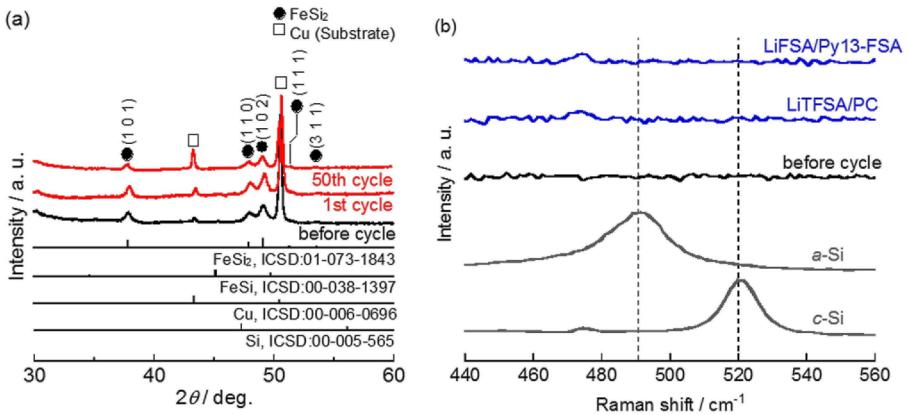

Figure 5. a) XRD patterns of lithiated $FeSi_2$ electrodes after 1 and 50 cycles in 1 M LiFSA/Py13-FSA. b) Raman spectra of delithiated $FeSi_2$ electrodes after the 10th cycle. The electrodes were cycled at 100 mA g^{-1}. The result before cycling is also shown.

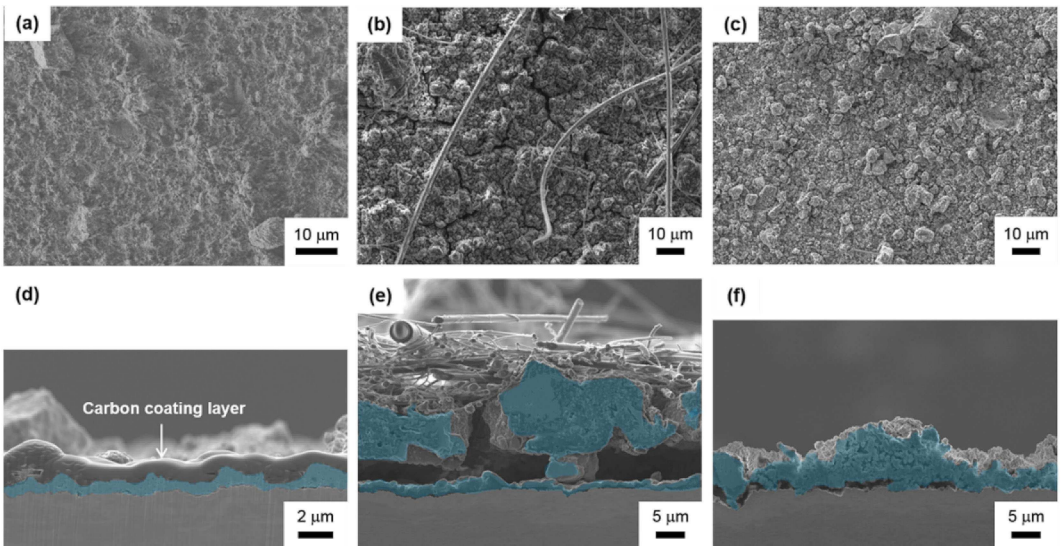

Figure 6. FE-SEM images of a–c) the surface and d–f) a cross-section of the $FeSi_2$ electrodes a, d) before and b, c, e, f) after the 100th charge process. The electrodes were cycled in b, e) organic and c, f) ionic liquid electrolytes at 100 mA g^{-1}, and these four images display lithiated $FeSi_2$ electrodes. Each blue area in (d)–(f) indicates the silicide layer. The fibers in (b) and (e) are part of the separator glass fibers. The cross-sections of (d) and (e, f) were processed by FIB and CP, respectively. A carbon coating layer protects the electrode surface against damage from the FIB process in part (d).

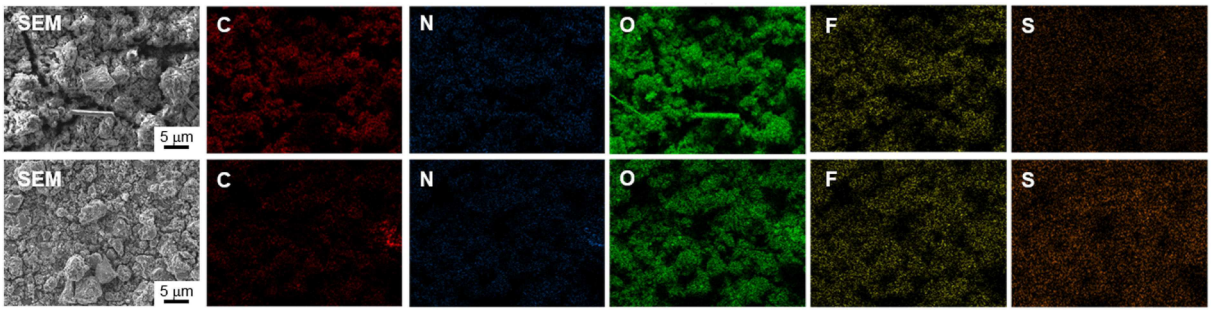

Figure 7. EDS mapping images of component involved in each electrolyte on lithiated $FeSi_2$ electrodes after 100 cycling in (upper) 1 M LiTFSA/PC and (lower) 1 M LiFSA/Py13-FSA. The electrodes were cycled at 100 mA g^{-1}.

electrodes after the 100th charge process (Figure S3). As a result, the lithiated $FeSi_2$ electrode maintains an OCV of ca. 0.15 V for approximately a week, which indicates that no self-discharge occurred. Before the charge-discharge tests, the electrode surface had no cracks and was smooth (Figure 6a). The thickness of pristine $FeSi_2$ electrode is estimated to be 0.9 ± 0.4 μm (Figure 6d). After the 100th cycle, micrometer–scale cracks are obviously observed in the organic electrolyte (Figure 6b). In contrast, in the ionic liquid electrolyte, large cracks did not form after the 100th cycle, whereas fine cracks are observed (Figure 6c). We also confirm several micrometer-sized aggregates. The $FeSi_2$ electrode thickness is estimated to be 14.0 ± 5.2 and 6.0 ± 3.1 μm in the organic and ionic liquid electrolytes, respectively (Figure 6e, f): the expansion of $FeSi_2$ is suppressed in the ionic liquid electrolyte. In addition, the active material layer of $FeSi_2$ exfoliates from the Cu current collector in the organic electrolyte. These results confirm the difference in the cycling performance of $FeSi_2$ electrode in both electrolytes.

Figure 7 shows energy-dispersive X-ray spectroscopy (EDS) mapping of the component involved in each electrolyte on the lithiated $FeSi_2$ electrode after the 100th cycle. Corresponding EDS mappings of other elements (Si and Fe) are also shown in Figure S4. In the organic electrolyte, fluorine, sulfur, and nitrogen were detected in addition to carbon and oxygen, which indicates that not only PC ($C_4H_6O_3$) but also LiTFSA ($C_2F_6LiNO_4S_2$) decompose on the electrode surface. On the other hand, in the ionic liquid electrolyte, carbon was hardly detected, and the other four elements were confirmed. This result demonstrates that the decomposition of the FSA anion ($F_2NO_4S_2$) occurs on the $FeSi_2$ electrode, whereas the Py13 cation ($C_8H_{18}N$) hardly decomposes. We previously reported that PC mainly decomposed on the cross-section of the Si-alone electrode, whereas no decomposition of LiTFSA occurred.[20] Therefore, the properties (component, thickness, and so on) of the surface films formed on different electrodes should differ even in the same electrolyte.

Figure 8 displays soft X-ray emission spectra of lithiated $FeSi_2$ electrodes and their corresponding FE-SEM images. While other methods cannot detect Li which is a light element, soft X-ray emission spectroscopy (SXES) is a powerful method for

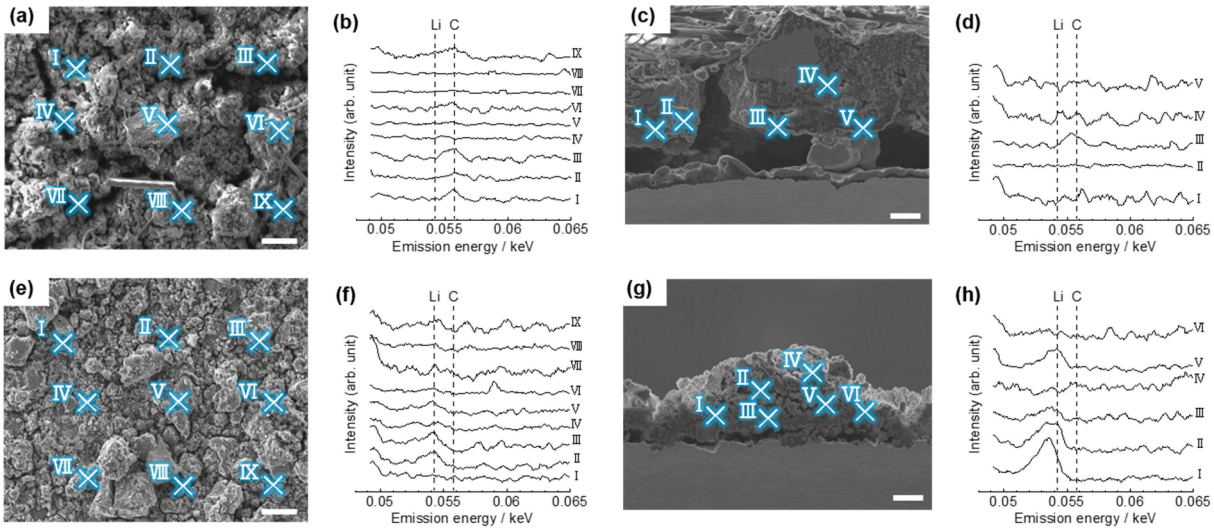

Figure 8. Li storage distribution. a, c, e, g) Cross-sectional FE-SEM and b, d, f, g) SXE spectra of the lithiated $FeSi_2$ electrodes in a–d) 1 M LiTFSA/PC and e–h) 1 M LiFSA/Py13-FSA. The crosses in the SEM image indicate the SXES measurement points, and the Roman numerals in the image correspond to those in the SXE spectrum. The electrodes were cycled at 100 mA g^{-1}.

elemental analysis because it can detect Li distribution by observing measurement points on SEM images. In SXE spectra, peaks assigned to lithium and carbon appear at 0.054 keV and 0.056 keV, respectively.[20] In the organic electrolyte, a carbon peak appears at some measurement points regardless of whether it is a surface or cross-section (Figure 8a–d). We also confirm the lack of peak for lithium. In contrast, in the ionic liquid electrolyte, the lithium peak and lack of carbon peak appear at many points in surface and cross-section (Figure 8e–h), which demonstrates that $FeSi_2$ itself reacts with Li. In addition, lack of detection of lithium in the organic electrolyte does not demonstrate that $FeSi_2$ does not react with Li based on the results of Figure 4a. It is considered that $FeSi_2$ loses the electronic continuity after the 100th cycle due to the exfoliation from the Cu current collector, as shown in Figure 6e.

3. Conclusions

We have reported the electrochemical lithiation and delithiation properties of some silicide anodes for LIBs in an ionic liquid electrolyte. The silicide electrodes have shown excellent cycle stability in an ionic liquid electrolyte, whereas they have exhibited a poor cyclability in a conventional organic electrolyte. The difference in the cycling performance results from the properties of the surface films formed on the electrodes in each electrolyte. Computational chemistry has revealed that a difference in the reversible capacity depending on the transition metals that make up the silicide is attributed to an affinity of the metal with Li. In addition, Cu_3Si and $FeSi_2$ electrodes exhibited high volumetric reversible capacity, which is superior to a Si-alone electrode. XRD and Raman spectroscopy have demonstrated that the crystal structure of the silicide is maintained during charge-discharge cycling, and no phase separation of silicide occurred. In the organic electrolyte, crack formation and exfoliation of the silicide from the Cu substrate occurred. In contrast, in the ionic liquid electrolyte, the crack formation and expansion of silicide layer were suppressed. EDS mapping revealed that the composition of the reductive decomposition product of the electrolyte on the $FeSi_2$ electrode differs from that on the Si-alone electrode. SXE spectra have demonstrated that $FeSi_2$ itself react with Li. The results obtained in this study will provide significant insights into novel alloy-based anode materials for LIBs.

Experimental Section

Synthesis of Various Silicide Powders

Silicide (M_ySi_z, *M*: metal) powders ($CrSi_2$, $Mn_{11}Si_{19}$, $FeSi_2$, $NiSi_2$, Cu_3Si and $LaSi_2$) were synthesized by a mechanical alloying (MA) method. Silicon (99.9%), manganese (98.0%), and iron (99.9%) powders were purchased from Wako Pure Chemical Industries, Ltd. Chromium (99.0%, NewMet Ltd.) nickel (99.9%, Nilaco Corp.), and copper (99.9%, Kojundo Chemical Laboratory Co., Ltd) powders were also used. A lanthanum chip (98.0%) supplied by Santoku Corp. was used after cutting it into smaller pieces. A mixture of elemental *M* and Si powders was put in a zirconia pod together with balls. An optimized mixture ratio, rotary speed and treatment time for each silicide are shown in Table 1. The weight ratio of the sample to the ball was approximately 1:15. The pod was filled with dry Ar gas. The MA was performed using a high-energy planetary ball mill (P-6, Fritsch).

Characterization

The obtained powders were characterized by X-ray diffraction (XRD, Ultima IV, Rigaku) and Raman spectroscopy (NanofinderFLEX; Tokyo Instruments, Inc.). XRD patterns were acquired at conditions of 40 kV and 40 mA with Cu–Kα radiation, and were identified compared with patterns in the Inorganic Crystal Structure Database (ICSD). XRD measurements were performed in air, except $LaSi_2$,

whereas $LaSi_2$ was covered with a polyimide film to prevent exposure to the atmosphere. Raman spectra were excited with the 532 nm line (16.5 mW) of a Nd:YAG laser at room temperature through a 50× objective lens. The scattered light was collected in a backscattering geometry. The Raman spectrum of $LaSi_2$ powder was obtained using a vessel that was not exposed to the atmosphere.

A cross-section of the electrode was observed by a field emission scanning electron microscope (FE-SEM, JSM-7800F, JEOL, Co., Ltd.) equipped with soft X-ray emission spectroscopy (SXES). The electrode was not exposed to the atmosphere until it was introduced into the FE-SEM chamber from cell disassembly using a transfer vessel. The acceleration voltage and working distance were set to 5 kV and 10 mm, respectively. A focused ion beam (FIB, JIB-4501, JEOL, Co., Ltd.) or cross-section polisher (CP, IB09020CP, JEOL, Co., Ltd.) was utilized to create the cross-section. The electrode surface was coated with carbon to protect it from damage by the Ga^+ beam of the FIB system.

Electrode Preparation and Charge-Discharge Test

Each silicide electrode was prepared by a gas deposition (GD) method, which does not require a binder or conductive agent.[41] The detailed conditions of GD were described in our previous paper.[7] The weight of the deposited active material was 30 ± 2 μg. We assembled 2032-type coin cells, which consisted of the silicide electrode as the working electrode, Li metal foil (Rare Metallic, 99.9%, thickness: 1 mm) as the counter electrode and a glass fiber filter (Whatman GF/A) as the separator. 1 mol dm^{-3} (M) lithium bis (fluorosulfonyl)amide (LiFSA) in *N*-methyl-*N*-propylpyrrolidinium bis (fluorosulfonyl)amide (Py13-FSA) was used as an ionic liquid electrolyte. For comparison, 1 M lithium bis(trifluoromethanesulfonyl)amide (LiTFSA) in propylene carbonate (PC, Kishida Chemical Co., Ltd.) was used as a conventional organic electrolyte. The $LaSi_2$ electrode preparation, cell (dis)assembly and electrolyte preparation were performed in an argon-filled glovebox (Miwa MFG, DBO-2.5LNKPTS) with a dew point below −100 °C.

A galvanostatic charge-discharge test was carried out using an electrochemical measurement system (HJ-1001SM8 A and HJ-1001SD8, Hokuto Denko Co., Ltd.) in the potential range between 0.005 and 2.000 V vs. Li^+/Li at 303 K. The current density was set at 50 mA g^{-1} unless otherwise stated. To analyze the reaction behaviors of silicide electrodes, XRD and Raman measurements were carried out after the charge-discharge cycling. The measurement conditions were the same as mentioned above. The electrode was protected by the polyimide film in the glovebox and sealed in the non-exposure vessel for XRD and Raman measurements, respectively, to prevent the electrode from reacting with air.

Computational Chemistry

To discuss the charge density distribution of each element in $Li_{0.25}M_ySi_z$ (M = Fe, Ni and La), a first-principle calculation based on density functional theory (DFT) was performed using the projector augmented wave (PAW) method as implemented in the plane wave code of the Vienna Ab initio Simulation Package (VASP).[42–46] A generalized gradient approximation (GGA) was used as the term exchange correlation with a kinetic cutoff of 350 eV. Brillouin zone sampling was performed with an 8×8×8 k point mesh within a Gamma point centered mesh scheme.

Acknowledgements

This work was partially supported by the Japan Society for the Promotion of Science (JSPS) KAKENHI (Grant Numbers JP17K17888, JP17H03128, JP16K05954) and the MEXT Program for Development of Environmental Technology using Nanotechnology.

Conflict of Interest

The authors declare no conflict of interest.

Keywords: lithium-ion batteries · silicide · ionic liquid electrolyte · gas deposition · soft X-ray emission spectroscopy

[1] M. S. Whittingham, *Chem. Rev.* **2004**, *104*, 4271–4301.
[2] M. Armand, J.-M. Tarascon, *Nature* **2008**, *451*, 652–657.
[3] B. Key, M. Morcrette, J.-M. Tarascon, C. P. Grey, *J. Am. Chem. Soc.* **2011**, *133*, 503–512.
[4] X. Zhou, Y.-X. Yin, A.-M. Cao, L.-J. Wan, Y.-G. Guo, *ACS Appl. Mater. Interfaces* **2012**, *4*, 2824–2828.
[5] M. T. McDowell, I. Ryu, S. W. Lee, C. Wang, W. D. Nix, Y. Cui, *Adv. Mater.* **2012**, *24*, 6034–6041.
[6] B. Liu, X. Wang, H. Chen, Z. Wang, D. Chen, Y.-B. Cheng, C. Zhou, G. Shen, *Sci. Rep.* **2013**, *3*, 1622.
[7] Y. Domi, H. Usui, M. Shimizu, Y. Kakimoto, H. Sakaguchi, *ACS Appl. Mater. Interfaces* **2016**, *8*, 7125–7132.
[8] B. R. Long, M. K. Y. Chan, J. P. Greeley, A. A. Gewirth, *J. Phys. Chem. C* **2011**, *115*, 18916–18921.
[9] H. Usui, M. Nomura, H. Nishino, M. Kusatsu, T. Murota, H. Sakaguchi, *Matter. Lett.* **2014**, *130*, 61–64.
[10] Y. Domi, H. Usui, Y. Takemoto, K. Yamaguchi, H. Sakaguchi, *J. Phys. Chem. C* **2016**, *120*, 16333–16339.
[11] G. A. Roberts, E. J. Cairns, J. A. Reimer, *J. Power Sources* **2002**, *110*, 424–429.
[12] Z. Du, T. D. Hatchard, P. Bissonnette, R. A. Dunlap, M. N. Obrovac, *J. Electrochem. Soc.* **2016**, *163*, A2456-A2460.
[13] Y. Yamada, K. Furukawa, K. Sodeyama, K. Kikuchi M. Yaegashi, Y. Tateyama, A. Yamada, *J. Am. Chem. Soc.* **2014**, 136, 5039–5046.
[14] J. Wang, Y. Yamada, K. Sodeyama, C. H. Chiang, Y. Tateyama, A. Yamada, *Nat. Commun.* **2016**, *7*, 12032.
[15] M. J. Earle, J. M. S. S. Esperança, M. A. Gilea, J. N. C. Lopes, L. P. N. Rebelo, J. W. Magee, K. R. Seddon, J. A. Widegren, *Nature* **2006**, *439*, 831–834.
[16] P. Hapiot, C. Lagrost, *Chem. Rev.* **2008**, *108*, 2238–2264.
[17] P. Sippel, P. Lunkenheimer, S. Krohns, E. Thoms, A. Loidl, *Sci. Rep.* **2015**, *5*, 13922.
[18] A. Ghoufi, A. Szymczyk, P. Malfreyt, *Sci. Rep.* **2016**, *6*, 28518.
[19] M. Shimizu, H. Usui, T. Suzumura, H. Sakaguchi, *J. Phys. Chem. C* **2015**, *119*, 2975–2982.
[20] K. Yamaguchi, Y. Domi, H. Usui, H. Sakaguchi, *ChemElectroChem* **2017**, *4*, 3257–3263.
[21] H. Usui, T. Masuda, H. Sakaguchi, *Chem. Lett.* **2012**, *41*, 521–522.
[22] H. Usui, M. Shimizu H. Sakaguchi, *J. Power Sources* **2013**, *235*, 29–35.
[23] F. M. Courtel, D. Duguay, Y. Abu-Lebdeh, I. J. Davidson, *J. Power Sources* **2012**, *202*, 269–275.
[24] G. X. Wang, L. Sun, D. H. Bradhurst, S. Zhong, S. X. Dou, H. K. Liu, *J. Power Sources* **2000**, *88*, 278–281.
[25] G. X. Wang, L. Sun, D. H. Bradhurst, S. Zhong, S. X. Dou, H. K. Liu, *J. Alloys Compds* **2000**, *306*, 249–252.
[26] A. Netz, R. A. Huggins, W. Weppner, *Ionics* **2001**, *7*, 433–439.
[27] M. D. Fleischauer, J. M. Topple, J. R. Dahn, *Electrochem. Solid-State Lett.* **2005**, *8*, A137–A140.
[28] M.-S. Park, Y.-J. Lee, S. Rajendran, M.-S. Song, H.-S. Kim, J.-Y. Lee, *Electrochim. Acta* **2005**, *50*, 5561–5567.
[29] W.-R. Liu, N.-L. Wu, D.-T. Shieh, H.-C. Wu, M.-H. Yang, C. Korepp, J. O. Besenhard, M. Winter, *J. Electrochem. Soc.* **2007**, *154*, A97–A102.

[30] Z. Du, S. N. Ellis, R. A. Dunlap, *M. N. Obrovac. J. Electrochem. Soc.* **2016**, *163*, A13–A18.
[31] Z. Du, H. Liu, S. N. Ellis, R. A. Dunlap, M. Zhu, *M. N. Obrovac. J. Electrochem. Soc.* **2016**, *163*, A1275–A1279.
[32] Z. Du, R. A. Dunlap, M. N. Obrovac, *J. Electrochem. Soc.* **2016**, *163*, A2011–A2016.
[33] Y. Cao, J. C. Bennett, R. A. Dunlap, *M. N. Obrovac. J. Electrochem. Soc.* **2018**, *165*, A1734–A1740.
[34] H. Cai, D. Tong, Y. Wang, X. Song, B. Ding, *J. Alloys Compd.* **2011**, *509*, 1672–1676.
[35] N. Nitta, G. Yushin, *Part. Part. Syst. Charact.* **2014**, *31*, 317–336.
[36] D. Ma, Z. Cao, A. Hu, *Nano-Micoro Lett.* **2014**, *6*, 347–358.
[37] L. Baggetto, J. F. M. Oudenhoven, T. van Dongen, J. H. Klootwijk, M. Mulder, R. A. H. Niessen, M. H. J. M. de Croon, P. H. L. Notten, *J. Power Sources* **2009**, *189*, 402–410.
[38] W.-J. Zhang, *J. Power Sources* **2011**, *196*, 13–24.
[39] C.-Y. Wen, F. Spaepen, *Philosophical Magazine*, **2007**, *87*, 5581–5599.
[40] T. D. Hatchard, J. R. Dahn, *J. Electrochem. Soc.* **2004**, *151*, A838-A842.
[41] H. Usui, Y. Kiri, H. Sakaguchi, *Thin Solid Films* **2012**, *520*, 7006–7010.
[42] G. Kresse, J. Furthmüller, *Phys. Rev. B* **1996**, *54*, 11169–11186.
[43] G. Henkelman, A. Arnaldsson, H. Jònsson, *Phys. Rev. B* **1999**, *59*, 1758–1775.
[44] P. Hapiot, C. Lagrost, *Comput. Mater. Sci* **2006**, *36*, 354–360.
[45] W. Tang, E. Sanville, G. Henkelman, *J. Phys. Condens. Matter* **2009**, *21*, 084204.
[46] E. Sanville, S. D. Kenny, R. Smith, G. Henkelman, *J. Comput. Chem.* **2007**, *28*, 899–908.

Manuscript received: August 7, 2018
Version of record online: October 31, 2018